Group Sparsity-Based Local Multipath Doppler Difference Estimation in Over-the-Horizon Radar

Vaishali S. Amin †, Yimin D. Zhang †, and Braham Himed ‡

† Department of Electrical and Computer Engineering, Temple University, Philadelphia, PA, 19122, USA
‡ RF Technology Branch, Air Force Research Laboratory, AFRL/RYMD, Dayton, OH, 45433, USA

***Abstract*—In sky-wave over-the-horizon radar systems, the received signal contains local multipath signal components as a result of reflection and refraction from ionosphere and the earth surface. For a maneuvering target, these multipath signals generally yield three distinct, yet closely separated, and highly time-varying Doppler components. Due to the proximity of these Doppler frequencies, it is a challenging task to accurately estimate the difference between these signatures, which reveal the important elevation velocity of the target. In this paper, we propose a group sparsity-based approach that exploits the correlation between these Doppler signatures and utilizes the *a priori* information about their characteristics. Simulation results verify the effectiveness of the proposed approach.**

***Index Terms*—Doppler frequency, group sparsity, over-the-horizon radar, target geo-location tracking, time-frequency analysis.**

I. Introduction

A traditional sky-wave over-the-horizon radar (OTHR) operates in the high-frequency (HF) band to detect targets that are located well beyond the limit of conventional line-of-sight radars by utilizing ionospheric reflections and refractions of the radar signals. OTHR performs wide-area surveillance, with a typical coverage of several thousand kilometers [1]. The narrow signal bandwidth constrained by the ionospheric conditions [2], along with other limiting conditions, such as low signal-to-noise ratio (SNR), and effective array aperture, adversely affect the range and cross-range resolutions of an OTHR system [3]. The range resolution of a typical skywave OTHR is measured in the order of tens of kilometers [3]. Due to the early warning nature of OTHR, high range resolution may not be required. However, high-resolution estimation of the target altitude, in the order of few kilometers or less, is needed for further target classification [4–6].

In practice, different multipath signals of a maneuvering target, generated due to the local multipath, i.e., reflections of the radar signal from the ocean/ground surface, along with ionospheric reflections, manifest themselves as distinct, yet closely separated, and highly time-varying Doppler frequency signatures. These Doppler signatures provide useful information for target geo-location, especially regarding the target's elevation velocity [7]. In the last two decades, various techniques, devised based on effective utilization of this local multipath model, have been proposed for maneuvering target detection and parameter estimation [4, 5, 8–10]. In an attempt to resolve these local multipath Doppler signatures, high-resolution time-frequency (TF) methods are employed [4, 5]. Nevertheless, due to the proximity of these non-linear Doppler components, it is not trivial to accurately obtain the difference between these components for accurate target altitude estimation. Besides, the existing techniques [4, 8–10] also suffer from high complexity due to the requirements of the exhaustive parametric analysis.

A low-complexity approach, which utilizes the prior information of these Doppler characteristics, is presented in [11]. In this approach, the squared magnitude of the received signal is first utilized to stationarize the nominal frequency component, leaving only the difference component of these Doppler signatures. Then, the short-time Fourier transform (STFT) [12, 13] is utilized to obtain the targeted Doppler frequency difference. While the method presented in [11] is effective in estimating the frequency difference when the difference Doppler frequency signatures are isolated, it does not yield accurate results particularly when multiple Doppler difference components are closely spaced. The low frequency resolution of the STFT for rapidly time-varying difference Doppler signatures is also a factor that compromises the estimation accuracy.

Recently, various sparse reconstruction-based TF analysis techniques [14–17] are shown to be effective in robust instantaneous frequency (IF) estimation of non-linear frequency modulated (FM) signals, which can be sparsely represented in the TF domain. We observe that, in the squared magnitude operation [11], the two difference Doppler components corresponding to the local multipath signals generate their harmonics, yielding four symmetrical components around the stationarized nominal Doppler frequency component. These four components are fully associated with the fundamental frequency as its negative frequency component and their harmonics. However, such group sparsity has not been considered in the context of OTHR local multipath signals.

Motivated by these observations, we propose a new group sparsity-based approach for effective Doppler difference estimation in this paper. We first remove the nominal Doppler component by using the squared magnitude of the received signal as in [11]. Then, we formulate the Doppler difference estimation as a group sparse reconstruction problem and design the dictionary that effectively represents the remaining components as the appropriate harmonics of the fundamental

The work of V. S. Amin and Y. D. Zhang is supported in part by a subcontract with Matrix Research, Inc. for research sponsored by the Air Force Research Laboratory under contract FA8650-14-D-1722.

frequency signature. The resulting problem is solved using one of the existing Bayesian compressive sensing-based group sparse reconstruction methods [18–21].

The key offering of the proposed method lies in that, by formulating the Doppler difference estimation as a group sparse reconstruction problem, the search space is reduced to one-fourth of the original search space for the multipath model considered in [4, 5, 10, 11], thus, greatly reducing the computational cost. At the same, the consideration of the four signal components that share a common sparse support would enhance the robustness and accuracy of their frequency estimation. The effectiveness of the proposed approach is verified through simulation results.

Notations. A lower (upper) case bold letter denotes a vector (matrix). $\mathbf{I}_N$ is the $N \times N$ identity matrix. $(\cdot)^{\mathrm{T}}$, $(\cdot)^{\mathrm{H}}$, and $(\cdot)^*$, respectively, denote transpose, Hermitian, and complex conjugation operations. $\mathrm{bdiag}(\cdot)$ represents a block diagonal matrix. $\mathrm{Tr}(\cdot)$ stands for matrix trace. $x \sim \mathcal{CN}(a, b)$ defines complex Gaussian distributed variable x, with mean a and variance b.

II. Signal Model

We consider a monostatic OTHR system with a flat-earth, local multipath propagation model [11] that assumes propagation through the stable E-layer of the ionosphere. This geometry is depicted in Fig. 1, where R and h are, respectively, the time-varying ground range and target altitude, whereas H is the height of the ionosphere which is considered constant over the processing interval and known from periodic ionosonde measurements. Note in Fig. 1 that the propagation paths and target below the ionosphere layer are the true ones, whereas those above the ionosphere layer are the equivalent of these paths, illustrated for computational convenience of the associated slant ranges.

From Fig. 1, the slant ranges associated with multipaths I and II are respectively given by

$$l_1 = \left(R^2 + (2H - h)^2\right)^{1/2}, \quad l_2 = \left(R^2 + (2H + h)^2\right)^{1/2}. \tag{1}$$

Since $h \ll H \ll R$ holds in practice, the slant ranges can be computed using the following approximations:

$$l_1 \approx R + \frac{2H^2 - 2Hh}{R}, \quad l_2 \approx R + \frac{2H^2 + 2Hh}{R}. \tag{2}$$

The horizontal and the vertical velocities of a maneuvering target are respectively defined as $\dot{R}(t) = \mathrm{d}R(t)/\mathrm{d}t$ and $\dot{h}(t) = \mathrm{d}h(t)/\mathrm{d}t$, where (t) is used to emphasize the time-dependency of the target parameters. From (2), we obtain

$$\begin{aligned} \frac{\mathrm{d}l_1(t)}{\mathrm{d}t} &\approx \dot{R}(t) - \frac{2H^2}{R^2(t)}\dot{R}(t) - \frac{2H}{R(t)}\dot{h}(t), \\ \frac{\mathrm{d}l_2(t)}{\mathrm{d}t} &\approx \dot{R}(t) - \frac{2H^2}{R^2(t)}\dot{R}(t) + \frac{2H}{R(t)}\dot{h}(t). \end{aligned} \tag{3}$$

The model presented in Fig. 1 has three unique propagation paths, created due to the local multipaths: (i) Mode I-I: when both transmit and receive signals follow path I, (ii) Mode II-II: when both transmit and receive signal follow path II, and (iii) Mode I-II: when the receive signal follows different path than the transmit signal (i.e., either path I-II or II-I). The associated Doppler frequencies of these three different propagation paths are, respectively, obtained as

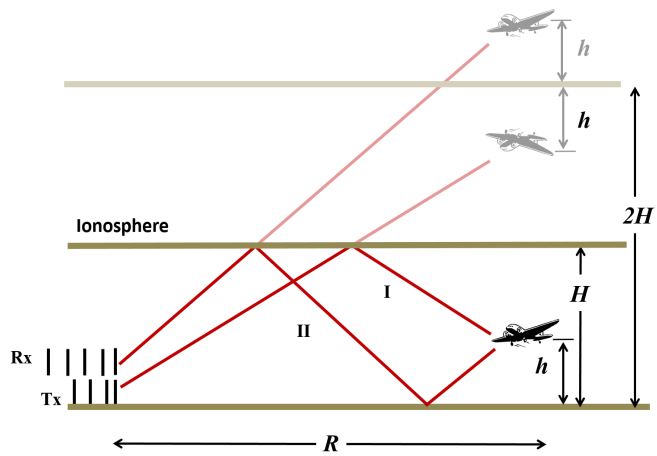

Fig. 1. Local multipath propagation model.

$$\begin{aligned} f_i(t) &= -\frac{2f_m}{c}\frac{\mathrm{d}l_1(t)}{\mathrm{d}t} \approx -\frac{2f_m}{c}B(t)\dot{R}(t) + \frac{4f_m H}{R(t)c}\dot{h}(t), \\ f_{ii}(t) &= -\frac{2f_m}{c}\frac{\mathrm{d}l_2(t)}{\mathrm{d}t} \approx -\frac{2f_m}{c}B(t)\dot{R}(t) - \frac{4f_m H}{R(t)c}\dot{h}(t), \\ f_{iii}(t) &= -\frac{f_m}{c}\frac{\mathrm{d}l_1(t) + \mathrm{d}l_2(t)}{\mathrm{d}t} \approx -\frac{2f_m}{c}B(t)\dot{R}(t), \end{aligned} \tag{4}$$

where f_m is the carrier frequency, c is the speed of the electromagnetic wave propagation, and for simplicity, we define $B(t) = 1 - 2H^2/R^2(t)$. It is clear from (4) that the Doppler frequencies for the first path and the second path are symmetric around that of the third path. Note that, in (4), the component $-2f_m B(t)\dot{R}(t)/c$ is shared by all three paths and carries an important information regarding the target velocity in the range direction. We refer to it as the nominal Doppler frequency, denoted as $f_N(t)$. Similarly, we represent the differential Doppler component as

$$f_D(t) = \frac{4f_m H\dot{h}(t)}{R(t)c}, \tag{5}$$

which revels an important information regarding elevation velocity, $\dot{h}(t)$, of a maneuvering target. Then, we can rewrite (4) as

$$\begin{aligned} f_i(t) &= f_N(t) + f_D(t), \\ f_{ii}(t) &= f_N(t) - f_D(t), \\ f_{iii}(t) &= f_N(t). \end{aligned} \tag{6}$$

From (4), it is clear that an accurate estimation of Doppler difference $f_D(t)$ plays a crucial role in target altitude estimation and tracking. However, the target altitude and its elevation velocity are, respectively, much smaller than the target range and its horizontal velocity. Hence, $f_D(t)$ is very small compared to $f_N(t)$, thus making its accurate estimation challenging, particularly for a maneuvering target with time-varying nominal Doppler frequency signatures.

Let a_n and $\theta_n(t)$, $n = 1, ..., 3$, respectively, be the magnitude and the instantaneous phase of the nth path. Then, the noise-free received signal can be expressed as

$$s(t) = \sum_{n=1}^{3} a_n \exp(j\theta_n(t)), \tag{7}$$

where the phase laws of the three unique multipaths are given by

$$\begin{aligned} \theta_1(t) &= -2\pi \textstyle\int_0^t f_i(t)\mathrm{d}t &= \phi(t) - \varphi(t), \\ \theta_2(t) &= -2\pi \textstyle\int_0^t f_{ii}(t)\mathrm{d}t &= \phi(t) + \varphi(t), \\ \theta_3(t) &= -2\pi \textstyle\int_0^t f_{iii}(t)\mathrm{d}t &= \phi(t), \end{aligned} \tag{8}$$

where $\phi(t) = 4\pi f_m B(t)R(t)/c$ and $\varphi(t) = 8\pi f_m Hh(t)/(R(t)c)$. Note that the change in $R(t)$ over the processing time is negligible, and thus it can be treated as a constant when obtaining the phase $\theta_n(t)$, $n = 1, ..., 3$. Due to the symmetry of Doppler signatures in (6), the sign of the Doppler difference cannot be obtained using local multipath-based approaches.

III. Doppler Difference Estimation through Group Sparse Reconstruction

Because of the small value of $f_D(t)$, it is often a challenging task to resolve the local multipath Doppler frequencies, particularly when the target is maneuvering, thus yielding nonlinearity in the Doppler signatures. In this section, we present a group sparsity-based method to accurately estimate the Doppler frequency difference. First, we use the squared magnitude of the received signal [11] to demodulate the Doppler signatures and remove the nominal Doppler component. Then, based on the prior knowledge of the characteristics of these Doppler signatures and their group sparsity, we formulate a group-sparse reconstruction problem, which is effectively solved using a block sparse Bayesian compressive sensing technique [19].

A. Demodulation of Doppler signatures

The stationarization-based TF analysis techniques presented in [4, 9] require highly time consuming processing of the data and often yield inaccurate estimation of the nominal Doppler frequency component. The self-demodulation technique, presented in [11], provides much simpler, yet more accurate Doppler signature demodulation without the need for a complicated nominal Doppler component estimation process. This procedure is summarized below.

The squared magnitude of the noiseless received signal, $s(t)$, can be obtained by multiplying it with its conjugate, as

$$\begin{aligned} |s(t)|^2 &= s(t)s^*(t) \\ &= \left(|a_1|^2 + |a_2|^2 + |a_3|^2\right) \\ &+ (a_1 a_3^* + a_2^* a_3)\exp(j\varphi(t)) \\ &+ (a_1^* a_3 + a_2 a_3^*)\exp(-j\varphi(t)) \\ &+ a_1 a_2^* \exp(j2\varphi(t)) + a_1^* a_2 \exp(-j2\varphi(t)). \end{aligned} \tag{9}$$

The operation in (9) yields four demodulated, localized frequency components, symmetrically located around the stationarized (i.e., DC) nominal Doppler component. As observed in (9), $|s(t)|^2$ does not contain $\phi(t)$. In order to obtain the elevation velocity of the maneuvering target, we only need to estimate $\varphi(t)$ from the Doppler signatures of $|s(t)|^2$ depicted in (9).

B. Group Sparse Reconstruction Problem Formulation

The resulting Doppler difference components in (9) are sparsely represented in the spectral domain. In order to estimate the differential Doppler component, we formulate it as a group sparse reconstruction problem as follows.

Denote $r(t) = s(t) + v(t)$ as the noisy received signal for $t = 1, \cdots, T$, where $v(t)$ denotes zero-mean complex white Gaussian noise. Let,

$$y(t) = |r(t)|^2 = |s(t)|^2 + |v(t)|^2 + \delta(t) = |s(t)|^2 + \Lambda(t), \tag{10}$$

where $\delta(t)$ accounts for the cross-terms between $s(t)$ and $v(t)$, and $\Lambda(t)$ represents combined effects of the noise and cross-terms. Without loss of generality, we refer to $\Lambda(t)$ as the noise terms. Define

$$\mathbf{y} = [y(1), \cdots, y(T)]^{\mathrm{T}}. \tag{11}$$

Dividing $\mathbf{y}$ into M overlapping segments, with N being the number of elements in each segment and Q being the frame hop, yields the following $N \times M$ matrix:

$$\mathbf{Y} = [\mathbf{y}_1, \mathbf{y}_2, ..., \mathbf{y}_M], \tag{12}$$

where

$$\mathbf{y}_m = [y((m-1)Q+1), ..., y((m-1)Q+N)]^{\mathrm{T}}. \tag{13}$$

From (9), it is clear that, other than the DC component, $\mathbf{y}_m$ comprises of four mutually associated frequency components, with one of them being the fundamental frequency, one being its mirrored negative frequency component, and the other two being their corresponding second-order harmonics. Using this information, we define the fundamental frequency vector as $\mathbf{f} = [f_1, f_2, ..., f_U]^{\mathrm{T}}$, where U represents the total number of fundamental frequencies. Consequently, the frequency vector of all possible frequencies, including harmonics, which contains U groups and a total number of $4U$ frequencies, is defined as

$$\tilde{\mathbf{f}} = [\mathbf{f}_1^{\mathrm{T}}, ..., \mathbf{f}_U^{\mathrm{T}}]^{\mathrm{T}}, \tag{14}$$

where

$$\mathbf{f}_u = [-2f_u, -f_u, f_u, 2f_u]^{\mathrm{T}}, \quad 1 \le u \le U, \tag{15}$$

represents a group of four frequencies related to the fundamental frequency f_u. Let

$$\tilde{\boldsymbol{\alpha}}_m = [\tilde{\boldsymbol{\alpha}}_1(m)^{\mathrm{T}}, ..., \tilde{\boldsymbol{\alpha}}_U(m)^{\mathrm{T}}]^{\mathrm{T}} \tag{16}$$

be the associated magnitude vector, which describes the Doppler difference spectrum of the signal, in the mth segment. Then, $\mathbf{y}_m$ can be expressed as the weighted sum of different frequencies plus noise terms. The group sparse reconstruction problem of $\mathbf{y}_m$ is formulated as

$$\mathbf{y}_m = \tilde{\boldsymbol{\Psi}}\tilde{\boldsymbol{\alpha}}_m + \tilde{\boldsymbol{\Lambda}}, \tag{17}$$

where $\tilde{\boldsymbol{\Psi}}$ is an $N \times 4U$ inverse Fourier transform matrix, given by

$$\tilde{\boldsymbol{\Psi}} = [\tilde{\boldsymbol{\Psi}}_1, ..., \tilde{\boldsymbol{\Psi}}_U], \tag{18}$$

and

$$\tilde{\mathbf{\Psi}}_u = \begin{bmatrix} 1 & 1 & 1 & 1 \\ e^{-2b} & e^{-b} & e^{b} & e^{2b} \\ \vdots & \vdots & \vdots & \vdots \\ e^{-2b(N-1)} & e^{-b(N-1)} & e^{b(N-1)} & e^{2b(N-1)} \end{bmatrix}, \quad (19)$$

where $b = j2\pi f_{nu}$ for some n that is associated with the specific fundamental Doppler frequency, $f_{nu} = f_u/f_w, 1 \leq u \leq U$, is the normalized frequency, and f_w is the pulse repetition frequency. Note that the amplitude $\tilde{\boldsymbol{\alpha}}_u(m), 1 \leq u \leq U$, and f_{nu}, are assumed to be time-invariant within each segment due to the consideration of a small time period.

Because the demodulated Doppler frequencies are sparsely represented in the TF domain, the solution vector $\tilde{\boldsymbol{\alpha}}_m$ is sparse, i.e., most of its blocks are zero. Ideally, in the absence of noise, other than the DC component, only one group of frequencies should assume a non-zero value for the entire segment. However, in practice, the estimation may contain few non-zero groups.

C. Group Sparse Reconstruction

While the group sparse reconstruction problem (17) can be solved using a number of group sparsity-based algorithms [18–23], Bayesian compressive sensing algorithms [18–21] generally provide superior results due to their adaptive learning framework. In this paper, we use the expectation maximization (EM)-based block sparse Bayesian learning (BSBL-EM) method [19] due to its proven superiority. The BSBL-EM was originally developed for real valued signals, and was extended for spectrum estimation of complex-valued harmonic speech signals [24]. The main steps of the algorithm in the context of our group sparse Doppler difference estimation problem are summarized below.

In the group sparse framework, each group $\tilde{\boldsymbol{\alpha}}_u(m) \in \mathbb{R}^{4\times 1}, 1 \leq u \leq U$, is assumed to satisfy the following parameterized multi-variate Gaussian distribution:

$$p\left(\tilde{\boldsymbol{\alpha}}_u(m); \lambda_u, \mathbf{C}_u\right) \sim \mathcal{CN}\left(\mathbf{0}, \lambda_u \mathbf{C}_u\right), \quad u = 1, \cdots, U, \quad (20)$$

where the unknown, non-negative parameter λ_u controls the block-sparsity of the solution vector $\tilde{\boldsymbol{\alpha}}_m$, whereas the unknown parameter $\mathbf{C}_u \in \mathbb{R}^{4\times 4}$ is a positive-definite matrix that captures the correlation structure of the uth block of $\tilde{\boldsymbol{\alpha}}_m$. As the solution vector comprises of only few blocks (ideally only one block in the underlying problem), λ_u assumes a zero value for most blocks. The prior of $\tilde{\boldsymbol{\alpha}}_m$ is given by

$$p\left(\tilde{\boldsymbol{\alpha}}_m; \{\lambda_u, \mathbf{C}_u\}_{u=1}^U\right) \sim \mathcal{CN}\left(\mathbf{0}, \mathbf{\Sigma}_0\right), \quad (21)$$

where $\mathbf{\Sigma}_0 = \mathrm{bdiag}\{\lambda_1 \mathbf{C}_1, ..., \lambda_{\mathrm{U}} \mathbf{C}_{\mathrm{U}}\}$. Assuming that the vector representing the noise terms satisfies $p(\tilde{\mathbf{\Lambda}}; \gamma) \sim \mathcal{CN}\left(\mathbf{0}, \gamma \mathbf{I}_N\right)$, where $\gamma > 0$, the posterior of $\tilde{\boldsymbol{\alpha}}_m$ is given by

$$p\left(\tilde{\boldsymbol{\alpha}}_m | \mathbf{y}_m; \gamma, \{\lambda_u, \mathbf{C}_u\}_{u=1}^U\right) = \mathcal{CN}\left(\boldsymbol{\mu}_{\alpha_m}, \mathbf{\Sigma}_{\alpha_m}\right), \quad (22)$$

where

$$\boldsymbol{\mu}_{\alpha_m} = \mathbf{\Sigma}_0 \tilde{\mathbf{\Psi}}^H \left(\gamma \mathbf{I}_N + \tilde{\mathbf{\Psi}} \mathbf{\Sigma}_0 \tilde{\mathbf{\Psi}}^H\right)^{-1} \mathbf{y}_m, \quad (23)$$

and

$$\mathbf{\Sigma}_{\alpha_m} = \left(\mathbf{\Sigma}_0^{-1} + \frac{1}{\gamma} \tilde{\mathbf{\Psi}}^H \tilde{\mathbf{\Psi}}\right)^{-1}. \quad (24)$$

TABLE I
KEY PARAMETERS

Parameter	Notation	Value
Initial range of target	$R(0)$	1,500 km
Height of ionosphere	H	160 km
Initial height of target	$h(0)$	10 km
Maximum range direction velocity	$v_{R,\max}$	175 m/s
Maximum elevation velocity	$v_{h,\max}$	19.68 m/s
Carrier frequency	f_m	16 MHz
Waveform repetition frequency	f_w	40 Hz

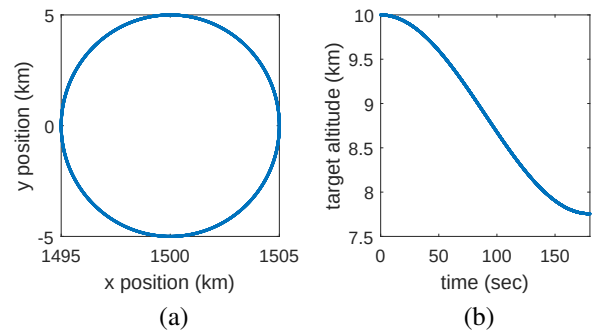

Fig. 2. Target parameters. (a) Target horizontal positions; (b) Target altitude.

Using the EM algorithm, the learning rules of λ_u and γ can be derived as:

$$\lambda_u \leftarrow \frac{1}{4} \mathrm{Tr}\left[\mathbf{C}_u^{-1}\left(\mathbf{\Sigma}_{\alpha_m}^u + \boldsymbol{\mu}_{\alpha_m}^u \left(\boldsymbol{\mu}_{\alpha_m}^u\right)^{\mathrm{T}}\right)\right], \; u = 1, \cdots, U, \quad (25)$$

$$\gamma \leftarrow \frac{\left\|\mathbf{y}_m - \tilde{\mathbf{\Psi}} \boldsymbol{\mu}_{\alpha_m}\right\|_2^2 + \sum_{u=1}^U \mathrm{Tr}\left(\mathbf{\Sigma}_{\alpha_m}^u \left(\tilde{\mathbf{\Psi}}_u\right)^{\mathrm{T}} \tilde{\mathbf{\Psi}}_u\right)}{N}. \quad (26)$$

It is worth noting that assigning a different $\mathbf{C}_u$ to each block may result in over-fitting [19]. In order to avoid that, parameter averaging is usually considered. This is achieved by constraining $\mathbf{C}_u = \mathbf{C}, \forall u$, provided that each block has the same size. Using this constraint and the EM algorithm, the learning rule for $\mathbf{C}$ can be derived as

$$\mathbf{C} \leftarrow \frac{1}{U} \sum_{u=1}^U \frac{\mathbf{\Sigma}_{\alpha_m}^u + \boldsymbol{\mu}_{\alpha_m}^u \left(\boldsymbol{\mu}_{\alpha_m}^u\right)^{\mathrm{T}}}{\lambda_u}. \quad (27)$$

After the parameters $\{\lambda_u, \mathbf{C}_u\}_{u=1}^U$ and γ are obtained, the maximum *a-posteriori* (MAP) estimate of $\tilde{\boldsymbol{\alpha}}_m$ is obtained as the mean of the posterior, given by

$$\hat{\boldsymbol{\alpha}}_m \leftarrow \mathbf{\Sigma}_0 \tilde{\mathbf{\Psi}}^H \left(\gamma \mathbf{I}_N + \tilde{\mathbf{\Psi}} \mathbf{\Sigma}_0 \tilde{\mathbf{\Psi}}^H\right)^{-1} \mathbf{y}_m. \quad (28)$$

IV. SIMULATION RESULTS

The effectiveness of the proposed method is verified through simulation results. We consider a maneuvering aircraft scenario [11] in which an aircraft makes a 360° circular turn of 5 km radius in approximately $T_0 = 179.5$ seconds, and descend by about 2.25 km. The horizontal velocity of the aircraft is assumed to be constant at 175 m/s, whereas its elevation velocity varies sinusoidally. The aircraft trajectory

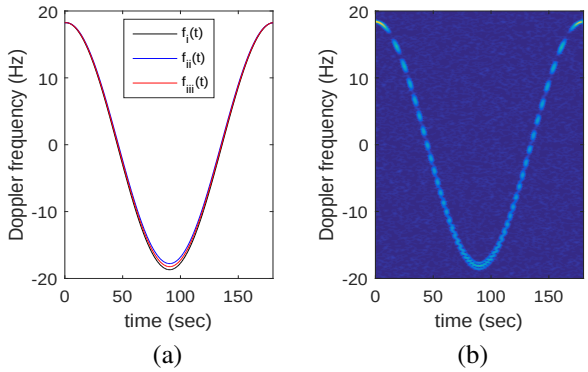

Fig. 3. Doppler signatures of $s(t)$. (a) True signatures; (b) Spectrogram.

is shown in Fig. 2. The other key parameters used in the simulations are provided in Table I. All local multipath signals are assumed to be the portion of the same range cell.

The time-varying altitude of a maneuvering target is given by

$$h(t) = h(0) - \frac{v_{h,\max} T_0}{\pi} \left[1 - \cos\left(\frac{\pi t}{T_0} \right) \right]. \tag{29}$$

The corresponding elevation velocity is obtained as

$$\dot{h}(t) = -v_{h,\max} \sin\left(\frac{\pi t}{T_0} \right). \tag{30}$$

From (5) and (30), it is clear that the differential Doppler component $f_D(t)$ is a function of $\dot{h}(t)$ and varies sinusoidally. The peak values of $f_D(t)$ and $f_N(t)$ are, respectively, obtained as 0.4478 Hz and 18.66 Hz, for the parameters considered in Table I. We assume that the clutter is filtered out using auto-regressive (AR) pre-whitening techniques [5, 25]. The effective input SNR after radar beamforming is set to 0 dB.

Fig. 3(a) shows multipath generated true Doppler frequency signatures. The corresponding spectrogram is shown in Fig. 3(b). It is clear that, due to proximity of these Doppler components and the time-varying nominal frequencies, the local multipath signals are not resolvable, making direct estimation of the Doppler frequency difference $f_D(t)$ challenging.

The true demodulated Doppler signatures, corresponding to $|s(t)|^2$, are shown in Fig. 4(a). Figs. 4(b) and 4(c), respectively, show the spectrogram and the Doppler TF signature obtained using the proposed approach, applied to the corresponding noisy signal $y(t) = |r(t)|^2$. In our simulations, the values of N, Q, M, and U are, respectively, taken as 512, 32, 210, and 201. Although the spectrogram in Fig. 4(b) catches the general trend of the time-varying Doppler frequency difference, the frequency resolution is poor. In particular, the harmonic components interfere to each other when the Doppler frequency difference is small. In Fig. 4(c), the result obtained using the proposed approach demonstrates high-resolution Doppler difference signatures and their robustness against harmonic interference and noise.

Fig. 5 describes the details of the proposed approach and provides a comparison with the existing result based on the spectrogram. Due to the symmetry of the harmonic Doppler difference signatures around the DC component, analysis of

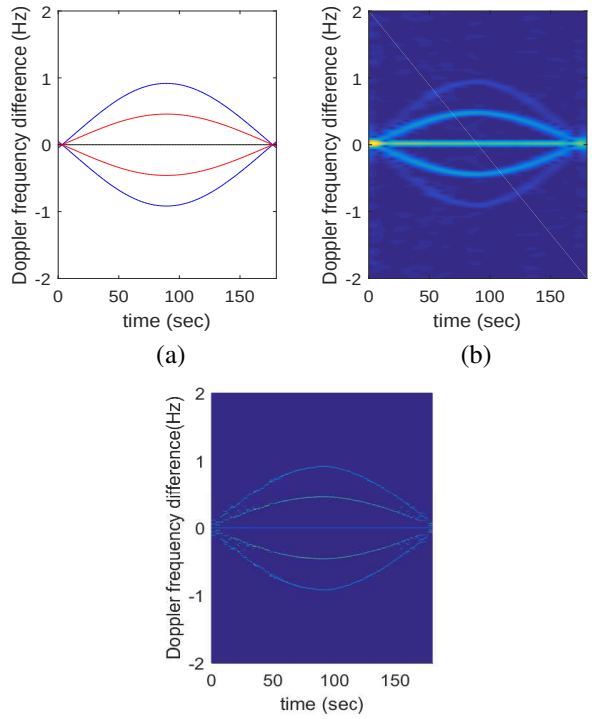

Fig. 4. Demodulated Doppler difference signatures. (a) True signatures; (b) Spectrogram; (c) Estimated signatures using the proposed method.

only the positive frequency side is required. The spectrogram depicted in Fig. 5(a) is obtained by fusing the Doppler signatures of the fundamental frequency and the harmonic frequency components [11], whereas Fig. 5(b) shows the corresponding estimate of the difference Doppler signature obtained using peak detection. Because the spectrogram depicted in Fig. 5(a) provides a low resolution and includes cross-terms between the fundamental and harmonic components, the peak detection results, as shown in Fig. 5(b), fail to provide accurate Doppler difference estimation in the first and the last 30 seconds of the observation period, where the Doppler difference is small. The TF representation of the estimated Doppler difference $f_D(t)$ is provided in Fig. 5(c), and the estimated difference Doppler signatures are plotted in Fig. 5(d). The root mean square error (RMSE) in terms of the normalized Doppler frequency using spectrogram and the proposed method are, respectively, obtained as 0.0282 and 0.0231. As such, both quantitative analysis and qualitative results confirmed the superiority of the proposed method in enhancing the frequency resolution and improving the robustness against noise.

V. Conclusion

In this paper, we developed a new group sparsity-based method to accurately estimate the Doppler frequency difference of the local multipath signals in OTHR systems. To achieve an accurate and robust estimation of this crucial information for determining the target elevation velocity, the proposed approach effectively utilizes the group sparsity between these frequencies and provides an improved estimation

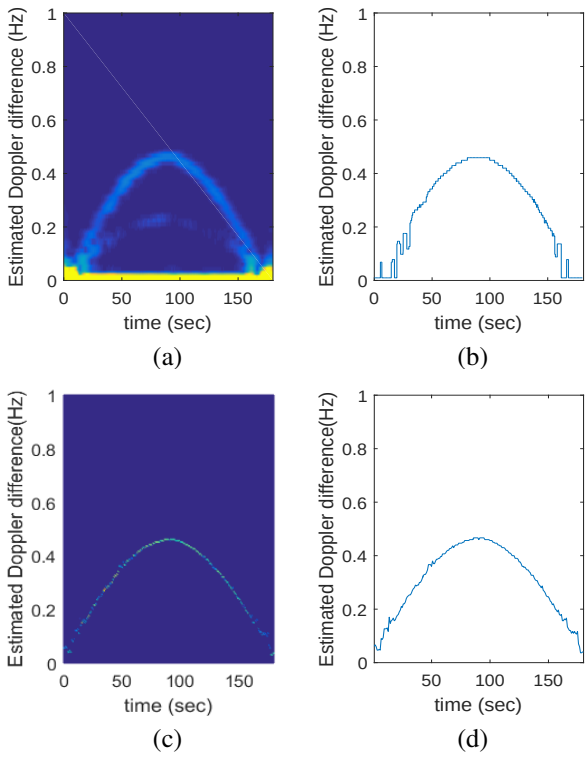

Fig. 5. The Estimated Doppler frequency difference, $f_D(t)$. (a) Spectrogram; (b) Peak detection result from spectrogram; (c) TF representation obtained from the proposed method; (d) Peak detection result from the proposed method.

result with a higher frequency resolution. Simulation results confirmed the effectiveness of the proposed technique, compared with existing methods.

References

[1] A. A. Kolosov (ed.), *Over-the-Horizon Radar*. Artech House, Boston, 1987.

[2] J. M. Headrick and S. J. Anderson, "HF over-the-horizon radar," Chapter 20 in M. Skolnik (ed.), *Radar Handbook, 3rd Ed.* McGraw-Hill, 2008.

[3] G. A. Fabrizio (ed.), *High Frequency Over-the-Horizon Radar: Fundamental Principles, Signal Processing, and Practical Applications*. McGraw-Hill, 2013.

[4] Y. D. Zhang, J. J. Zhang, M. G. Amin, and B. Himed, "Instantaneous altitude estimation of maneuvering targets in over-the-horizon radar exploiting multipath Doppler signatures," *EURASIP J. Adv. Signal Process.*, vol. 2013, no. 2013:100, pp. 1–13, May 2013.

[5] Y. Zhang, M. G. Amin, and G. J. Frazer, "High-resolution time-frequency distributions for manoeuvring target detection in over-the-horizon radars," in *Proc. IEE Radar Sonar Navig.*, vol. 150, no. 4, Nov. 2003, pp. 299–304.

[6] Y. D. Zhang, M. G. Amin, and B. Himed, "Altitude estimation of maneuvering targets in MIMO over-the-horizon radar," in *Proc. IEEE Sensor Array Multichannel Signal Process. Workshop (SAM)*, Hoboken, NJ, June 2012, pp. 257–260.

[7] R. H. Anderson, S. Kraut, and J. L. Krolik, "Robust altitude estimation for over-the-horizon radar using a state-space multipath fading model," *IEEE Trans. Aerospace Electron. Syst.*, vol. 39, no. 1, pp. 192–201, Jan. 2003.

[8] C. Ioana, M. G. Amin, Y. D. Zhang, and F. Ahmad, "Characterization of Doppler effects in the context of over-the-horizon radar," in *Proc. IEEE Radar Conf.*, Washington, D.C., May 2010, pp. 506–510.

[9] C. Ioana, Y. D. Zhang, M. G. Amin, F. Ahmad, G. Frazer, and B. Himed, "Time-frequency characterization of micro-multipath signals in over-the-horizon radar," in *Proc. IEEE Radar Conf.*, Atlanta, GA, May 2012, pp. 671–675.

[10] I. Djurovic, S. Djukanovic, M. G. Amin, Y. D. Zhang and B. Himed, "High-resolution time-frequency representations based on the local polynomial Fourier transform for over-the-horizon radars," in *Proc. SPIE Defense Security Sensing Conf.*, vol. 8361, Baltimore, MD, May 2012.

[11] Y. D. Zhang and B. Himed, "Multipath Doppler difference estimation in over-the-horizon radar," *IEEE Radar Conf.*, Oklahoma City, OK, Apr. 2018, pp. 0693–0697.

[12] L. Cohen, *Time-Frequency Analysis*. Prentical Hall, 1995.

[13] V. Chen and H. Ling, *Time-Frequency Transforms for Radar Imaging and Signal Analysis*. Aetech House, 2002.

[14] V. S. Amin, Y. D. Zhang, and B. Himed, "Sparsity-based time-frequency representation of FM signals with burst missing samples," *Signal Process.*, vol. 155, pp. 25–43, Feb. 2019.

[15] V. S. Amin, Y. D. Zhang, and B. Himed, "Improved instantaneous frequency estimation of multi-component FM signals," in *Proc. IEEE Radar Conf.*, Boston, MA, Apr. 2019.

[16] V. S. Amin, Y. D. Zhang, and B. Himed, "Sequential time-frequency signature estimation of multi-component FM signals," in *Proc. IEEE Asilomar Conf. Signals Syst. Comp.*, Pacific Grove, CA, Nov. 2019.

[17] S. Zhang and Y. D. Zhang, "Robust time-frequency analysis of multiple FM signals with burst missing samples," *IEEE Signal Process. Lett.*, vol. 26, no. 8, pp. 1172–1176, June 2019.

[18] S. Ji, D. Dunson, and L. Carin, "Multitask compressive sensing," *IEEE Trans. Signal Proc.*, vol. 57, no. 1, pp. 92-106, Jan. 2009.

[19] Z. Zhang and B. D. Rao, "Extension of SBL algorithms for the recovery of block sparse signals with intrablock correlation," *IEEE Trans. Signal Process.*, vol. 61, no. 8, pp. 2009–2015, Apr. 2013.

[20] Q. Wu, Y. D. Zhang, M. G. Amin, and B. Himed, "Complex multitask Bayesian compressive sensing, in *Proc. IEEE Int. Conf. Acoustics, Speech, Signal Process.*, Florence, Italy, May 2014, pp. 3375–3379.

[21] Q. Wu, Y. D. Zhang, M. G. Amin, and B. Himed, "Multi-task Bayesian compressive sensing exploiting intra-task correlation," *IEEE Signal Process. Lett.*, vol. 22, no. 4, pp. 430–434, Apr. 2015.

[22] Y. Eldar, P. Kuppinger, and H. Bolcskei, "Block-sparse signal: uncertainty relations and efficient recovery," *IEEE Trans. Signal Process.*, vol. 58, no. 6, pp. 3042–3054, June 2010.

[23] L. Jacob, G. Obozinski, and J. Vert, "Group Lasso with overlap and graph Lasso," in *Proc. Int. Conf. Mach. Learn.*, Montreal, QC, June 2009.

[24] Y. D. Zhang and B. Wang, "Group sparsity based estimation of harmonic speech signals," in *Proc. SPIE Compressive Sensing Conf.*, vol. 9484, Baltimore, MD, May 2015.

[25] T. J. Nohara and S. Haykin, "AR-based growler detection in sea clutter," *IEEE Trans. Signal Process.*, vol. 41, no. 3, pp. 1259–1271, Mar. 1993.